

## Article

# Multi-Objective Optimization Design of 6-UPS Parallel Mechanism Based on Taguchi Method and Entropy-Weighted Gray Relational Analysis

Hao Song <sup>1</sup>, Xiaoliang Chen <sup>1,2</sup>, Shuai Zhang <sup>1</sup> and Liyou Xu <sup>1,\*</sup>

<sup>1</sup> College of Vehicle and Traffic Engineering, Henan University of Science and Technology, Luoyang 471003, China; car\_sh@163.com (H.S.); cxl\_cn@163.com (X.C.); boreke@126.com (S.Z.)

<sup>2</sup> School of Vehicle and Traffic Engineering, Henan Institute of Technology, Xinxiang 453000, China

\* Correspondence: xlyou@haust.edu.cn

**Abstract:** Nowadays, parallel mechanisms are widely used in many fields because of their excellent structural performance. In order to improve the comprehensive performance of 6-UPS parallel mechanism, this article proposes a multi-objective optimization design method for parallel mechanism based on the Taguchi method and entropy-weighted gray relational analysis (EGRA) method. By establishing a parametric model of the 6-UPS parallel mechanism, taking the peak force on the drive pair of the drive branch chain of the mechanism, the minimum value of the projection angle of the body-fixed coordinate system (BCS) relative to the inertial coordinate system (ICS), and the minimum value of the average projected angle of the BCS relative to the ICS as the objective functions, the relationship between the design variables and the objective function is investigated under the condition that the constraints are satisfied. Using the optimization method proposed in this article, the multi-objective optimization problem is transformed into a single-objective optimization problem based on gray relational grade (GRG). Compared with the non-optimized 6-UPS parallel mechanism, the simulation results show that the peak force on the drive pair of the drive branch chain is reduced by 17.73%, and the minimum value of the projected angle and the minimum value of the average projected angle of the BCS relative to the ICS are increased by 27.36% and 36.17%, respectively, which effectively improves the load-bearing capacity and motion range of the 6-UPS parallel mechanism and verifies the reliability of the optimized design method.

**Keywords:** 6-UPS parallel mechanism; Taguchi method; entropy-weighted gray relational analysis; factor effect analysis; multi-objective optimization



**Citation:** Song, H.; Chen, X.; Zhang, S.; Xu, L. Multi-Objective Optimization Design of 6-UPS Parallel Mechanism Based on Taguchi Method and Entropy-Weighted Gray Relational Analysis. *Appl. Sci.* **2022**, *12*, 5836. <https://doi.org/10.3390/app12125836>

Academic Editors: Chang Yong Song and Wu Deng

Received: 21 April 2022

Accepted: 7 June 2022

Published: 8 June 2022

**Publisher's Note:** MDPI stays neutral with regard to jurisdictional claims in published maps and institutional affiliations.



**Copyright:** © 2022 by the authors. Licensee MDPI, Basel, Switzerland. This article is an open access article distributed under the terms and conditions of the Creative Commons Attribution (CC BY) license (<https://creativecommons.org/licenses/by/4.0/>).

## 1. Introduction

With the advantages of simple structure, high positioning accuracy, and fast dynamic response, the parallel mechanism has been extensively used in the fields of advanced manufacturing equipment, national defense and military, automobile manufacturing, aerospace, and motion simulation [1–3]. In previous studies, researchers have explored parallel mechanisms from various aspects, especially in structural synthesis and design theory [4–6], kinematics and dynamics studies [7–9], singularity analysis [10–12], operation mode studies [13,14], and efficient control strategies [15,16]. These studies provide a deep foundation for the development of parallel mechanisms.

The main body of the 6-UPS parallel mechanism is composed of a mobile platform, a fixed platform, and six drive branch chains, where U stands for universal joint, P stands for prismatic pair, and S stands for spherical hinge. The 6-UPS parallel mechanism performance and its structural parameters are closely related. When the structural parameters are unreasonably designed, the mechanism's performance will be significantly reduced. Therefore, researchers have also been working on the optimization design of the structure and performance of parallel mechanism, where the most commonly used optimization methods

are divided into two categories: optimization methods based on objective functions and optimization methods based on performance atlas [17–19].

The optimization method based on objective function is to build up the objective function and constraints according to the optimization index and then use the optimization algorithm to search for the optimal solution. The optimization methods based on objective function are mostly used in the case of many parameter variables and too complex objective function. When there are two or more objective functions, it is called a multi-objective optimization problem, and solving a multi-objective optimization problem is a process of finding the Pareto optimal solution [20–22]. Qi et al. [23] conducted a multi-objective optimization of a typical parallel tracking mechanism under comprehensive consideration of the kinematics, stiffness, workspace, and dynamic performances, while considering manufacturing and assembly errors. Zhang et al. [24] used the PSO algorithm to perform multi-objective optimization of the workspace, dexterity, stiffness, energy efficiency, motion/force transfer efficiency, and inertial coupling index of the established 2RPU-2SPR super-constrained redundantly driven parallel mechanism. Mirshekari et al. [25] studied the effects of different parameters, such as the rotation joint angle and spherical joint position of the 6-RUS parallel robot mobile platform on the workspace, kinematics and dynamics indices, and they used the bees algorithm approach to optimize the manipulator structure.

The optimization method based on performance atlas refers to intuitively expressing the relationship between design indices and design parameters in a limited design space, so as to obtain the performance atlas of the mechanism. Liu and Wang [26] optimized the 3PRS mechanism and the spherical 5R parallel mechanism with 2-DOF by using the performance atlas method, so that they had better kinematic performance and force transmission performance in the workspace. Pan and Hou [27] conducted a comprehensive study on a mobile complex multi-body system, through mechanism analysis and identification, introducing sensitivity analysis and extracting key design variables from global variables for multi-objective optimization design. Wang et al. [28] took the motion/force transmissibility and the workspace range as the optimization objectives, respectively, expressing the relationship between the corresponding motion indices and structural parameters by using the performance atlas method and realized the optimal design of 3-PUU mechanism. However, there is a problem in the optimization method based on performance atlas, that is, when there are many characteristic parameters to be optimized, it cannot completely represent the performance atlas in a limited space.

In recent years, the approximate model technology has developed rapidly in multi-objective optimization [29,30]. By fitting the mathematical relationship between input and output, the approximate model technology can replace the real value with the predicted value of the approximate model within a certain error range, so as to effectively improve the calculation efficiency and simulation accuracy [31,32]. The widely used approximate models in engineering mainly include response surface method surrogate model, Kriging surrogate model, and radial basis function surrogate model [33,34]. Hu et al. [35] developed a Latin hypercube design, Kriging interpolation, and neural network training (LKN) method based on the response surface method, taking into account both kinematic and dynamic performance indices, carrying out the robustness design of the 4PUS-1RPU parallel mechanism.

The Taguchi method was initially created for quality engineering to assess and produce better robustness, tolerance specification, and quality management of production processes [36]. The Taguchi method does not rely on complex probabilistic or statistical analysis. It can mine the information of the whole parameter space through a little number of experiments to obtain the optimal solution of the experimental design [37,38]. Park et al. [39] performed kinematic optimization of a redundantly driven parallel mechanism using the Taguchi method with the optimization objective of maximizing the total of energy efficiency and workspace. Wu et al. [40] used the Taguchi method and Monte Carlo simulation method to optimize the 3-RRR parallel micro-movement platform iteratively

and found the optimal geometric size of the flexure hinge. Shin et al. [41] proposed an optimization method using the Taguchi method to optimize the redundantly driven parallel mechanism by studying the kinematic parameters of a planar 2-DOF parallel robot; the optimal parameter combination between the link length and stiffness was obtained.

The multi-objective optimization design problem is driven by many competitive standards, and although optimization algorithm can provide designers with a large number of non-dominated optimal solutions, designers still need to use engineering knowledge to independently choose the best compromise solution [42]. Gray correlation analysis (GRA) has been widely used in various decision-making problems. Its basic idea is to use the linear interpolation between adjacent points of the sequence to map the discrete data to the geometry of the space and to determine the correlation between the sequences by calculating the distance between the reference sequence and the comparison sequence [43,44]. Dao and Huang [45,46] used optimization techniques, such as the Taguchi method, response surface method, GRA, and entropy weight measurement, to carry out a multi-objective optimization design for the 2-DOF flexible mechanism and the 2-DOF flexible mechanism with a modified double-lever amplification mechanism, respectively. Hsieh et al. [47] used the GRA method to design the mechanical structure of the conical guide mechanism to solve the interference misalignment problem during excavator attachment assembly.

However, traditional optimization methods are generally only suitable for linear and simple systems, and when they are applied to multi-objective optimization problems, there will be some limitations, such as difficulty in solving and global optimal solutions being ignored [48]. Although intelligent optimization methods outperform traditional optimization methods in solving multi-objective problems, they also have their own limitations, such as being time consuming and having poor convergence [49]. In order to solve this problem, many scholars try to develop new optimization methods, among which the hybrid algorithm can better combine the optimization efficiency and accuracy, so as to solve the multi-objective optimization problem [50,51]. In addition, it also has great application prospects in multi-objective optimization design by combining multiple optimization methods. Wang et al. [52] proposed an optimization method combining radial basis function neural network model, fuzzy subtractive clustering sequential sampling method, and NSGA-II, which is used to improve the calculation efficiency and accuracy of multi-objective optimization problems in engineering. Xiong et al. [53] proposed a hybrid method combining contribution analysis, radial basis function neural-network-response surface method hybrid surrogate modeling method, and PSO algorithm for lightweight design of body front-end structures.

The above studies have carried out multi-objective optimization design of parallel mechanism from different aspects, such as the optimization method based on objective function, optimization method based on performance atlas, approximate model technology, Taguchi method, and gray relational analysis method. In order to further improve the optimization efficiency of the parallel mechanism, on the basis of the above research, this article conducts a multi-objective optimization design of the 6-UPS parallel mechanism based on the parametric modeling technology, the Taguchi method, and entropy-weighted gray relational analysis (EGRA) method. The parametric model of a 6-UPS parallel mechanism is established by ADAMS software, and the validity and accuracy of the parametric model are verified by theoretical calculation. By studying the association between the design variables and the objective function, the multi-objective optimization problem of parallel mechanism is transformed into a single-objective optimization problem based on the gray relational grade (GRG) by using the EGRA method to realize the multi-objective optimal design of the load-bearing capacity and motion range of the 6-UPS parallel mechanism.

## 2. Multi-Objective Optimization Design Method

Based on parametric modeling technology, the Taguchi method, and the EGRA method, the optimization design of 6-UPS parallel mechanism in this article is mainly divided into five steps, and the optimization design process is shown in Figure 1.

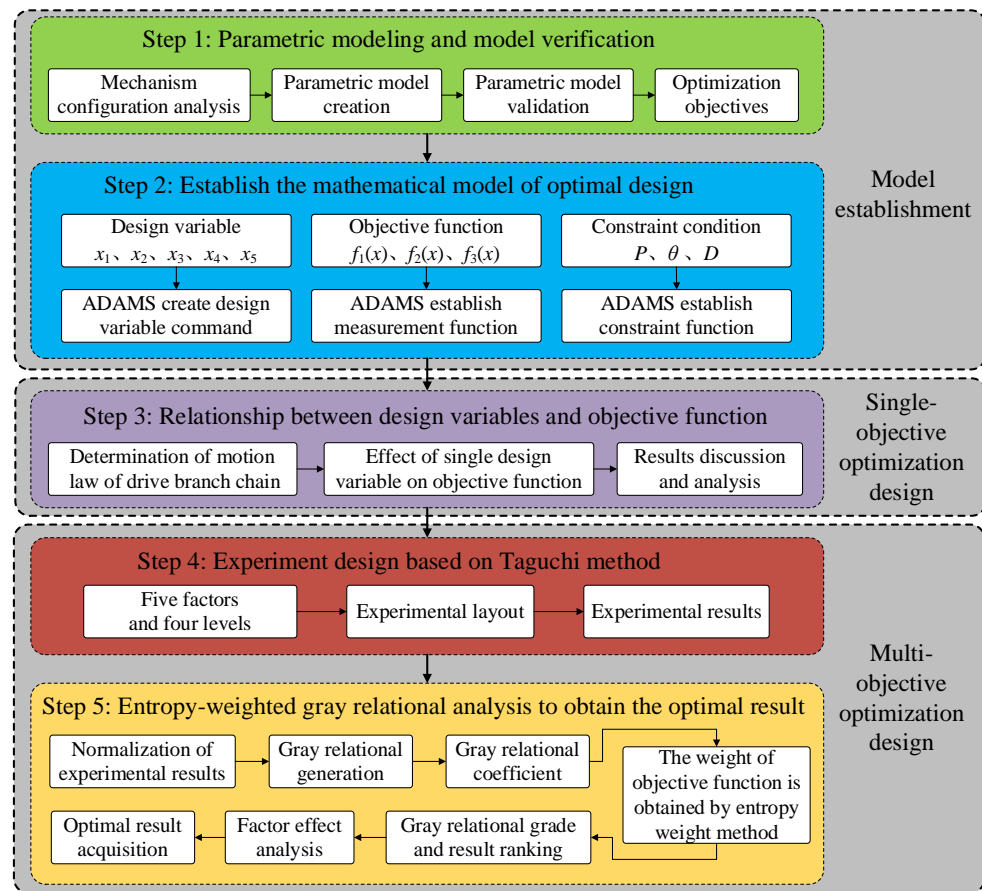


Figure 1. Optimization design process.

Step 1: Parametric modeling and model validation. The key factors affecting the structural performance of 6-UPS parallel mechanism are found out through the mechanism configuration analysis, and then, the parametric model of the mechanism is created in ADAMS software, and the validity and accuracy of the parametric model are verified by comparing the simulation and theoretical calculation results.

Step 2: Establishing the mathematical model of optimal design. According to the structural parameters and expected structural performance of 6-UPS parallel mechanism, the mathematical models of design variables, objective functions, and constraints are created, and the corresponding design functions are established in ADAMS software.

Step 3: Research on the relationship between design variables and objective functions. By creating the motion law of the driving branch chain, the effect of a single design variable on the objective function is studied, so as to facilitate the subsequent transformation of the multi-objective problem into a single-objective optimization problem.

Step 4: Experiment design based on the Taguchi method. By studying the effect of a single design variable on the objective function, five factors and four levels are determined, and the experimental layout and optimization are carried out by the Taguchi method.

Step 5: EGRA obtains the optimal result. The GRG of each scheme in the Taguchi experimental design is obtained by GRA, and the optimization results are sorted. The average GRG of each design variable is obtained by factor effect analysis, and the optimal result is obtained.

### 3. Parametric Modeling and Model Validation

#### 3.1. 6-UPS Parallel Mechanism Configuration Analysis

The 6-UPS parallel mechanism comprises a mobile platform, a fixed platform, drive branch chains, spherical hinge, and universal joint. Among them, the fixed platform is

set on the base, the telescopic rod end of the drive branch chains is linked to the mobile platform by the spherical hinge, the cylinder end is linked to the fixed platform by the universal joint, and the drive branch chains are used as the driving input device of the mechanism, which enables the mobile platform to complete 6-DOF of movement in space through its respective independent telescopic movements: lateral movement, longitudinal movement, vertical movement, pitch, roll, and yaw.

The structure of the 6-UPS parallel mechanism is shown in Figure 2. Among them,  $A_i$  represents the position of the six spherical hinges;  $B_i$  represents the position of the six universal joints;  $r$  is the distribution circle radius of the geometric center of the spherical hinge of the mobile platform;  $R$  is the distribution circle radius of the geometric center of the universal joint of the fixed platform;  $\alpha$  is the central angle corresponding to the long side of the spherical hinge;  $\beta$  is the central angle corresponding to the short side of the universal joint;  $H$  is the initial height between the center point  $O_a$  of the mobile platform and the center point  $O_b$  of the fixed platform.

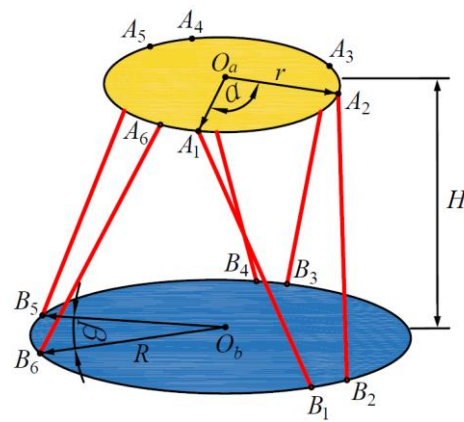


Figure 2. Structure of the 6-UPS parallel mechanism.

### 3.2. Parametric Model Creation

The parametric model of the 6-UPS parallel mechanism is established by ADAMS software. The parametric model is based on parameterizing the point coordinates, and the model can be updated automatically by changing only the parameters of the design variables when modifying the model, so as to research the relevant performance of the parallel mechanism under various parameters. The parameterized point coordinates of the mechanism are shown in Table 1.

Table 1. Parameterized point coordinates of the 6-UPS parallel mechanism.

Parametric Point	X Coordinate	Y Coordinate	Z Coordinate
$A_1$	$r \cos (\alpha / 2)$	$-r \sin (\alpha / 2)$	$H$
$A_2$	$r \cos (\alpha / 2)$	$r \sin (\alpha / 2)$	$H$
$A_3$	$r \cos (120^\circ - \alpha / 2)$	$r \sin (120^\circ - \alpha / 2)$	$H$
$A_4$	$r \cos (120^\circ + \alpha / 2)$	$r \sin (120^\circ + \alpha / 2)$	$H$
$A_5$	$r \cos (120^\circ + \alpha / 2)$	$-r \sin (120^\circ + \alpha / 2)$	$H$
$A_6$	$r \cos (120^\circ - \alpha / 2)$	$-r \sin (120^\circ - \alpha / 2)$	$H$
$B_1$	$R \cos (\beta / 2)$	$-R \sin (\beta / 2)$	$0$
$B_2$	$R \cos (\beta / 2)$	$R \sin (\beta / 2)$	$0$
$B_3$	$R \cos (120^\circ - \beta / 2)$	$R \sin (120^\circ - \beta / 2)$	$0$
$B_4$	$R \cos (120^\circ + \beta / 2)$	$R \sin (120^\circ + \beta / 2)$	$0$
$B_5$	$R \cos (120^\circ + \beta / 2)$	$-R \sin (120^\circ + \beta / 2)$	$0$
$B_6$	$R \cos (120^\circ - \beta / 2)$	$-R \sin (120^\circ - \beta / 2)$	$0$

After the parametric points are created, the corresponding structural components are produced according to Figure 2; the spherical pair and the universal pair are added to the

spherical hinge and the universal joint, respectively, and the moving pair is added to the drive branch chain. The parametric model of the mechanism created is shown in Figure 3.

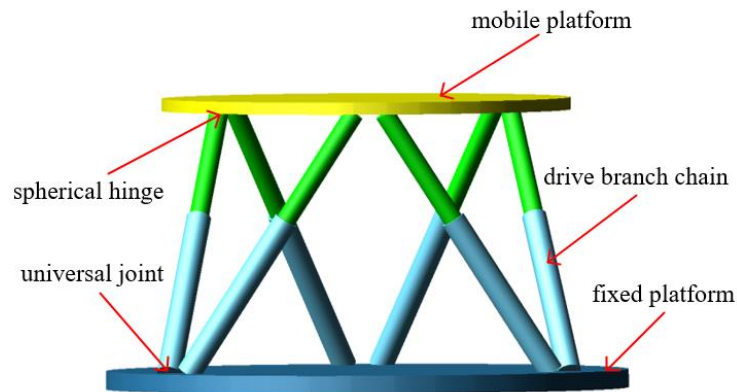


Figure 3. Parametric model of the 6-UPS parallel mechanism.

### 3.3. Parametric Model Validation

Although the structural parameters of the model can be changed quickly through parametric modeling, unverified models can lead to unreliable designs. Therefore, it is essential to compare the simulation test results with the theoretical calculation results to verify the validity of the parametric model before the optimization design is carried out.

Selecting the drive branch chain as the research object, when the distribution circle radius  $r$  of the geometric center of the spherical hinge of the mobile platform and the distribution circle radius  $R$  of the geometric center of the universal joint of the fixed platform are known, the position vector  $A_i$  at the connection between the mobile platform and the spherical hinge and the position vector  $B_i$  at the connection between the fixed platform and the universal joint can be represented on the respective coordinate systems to determine the length vector  $L_i$  of the drive branch chain.

$$L_i = RA_i + E_i - B_i \quad (i = 1, 2, \dots, 6) \tag{1}$$

where  $L_i$  is the length vector of the drive branch chain;  $R$  is the rotation transformation matrix obtained after three rotation transformations;  $A_i$  is the position vector at the connection between the mobile platform and the spherical hinge;  $E_i$  is the unit matrix;  $B_i$  is the position vector at the connection between the fixed platform and the universal joint.

The coordinate transformation diagram of the mechanism is shown in Figure 4. Among them, the body-fixed coordinate system (BCS)  $O_a-X_aY_aZ_a$  on the mobile platform can be regarded as obtained by the inertial coordinate system (ICS)  $O_b-X_bY_bZ_b$  on the fixed platform after three translations and three rotations.

The ICS is translated in the order along the  $X$  axis,  $Y$  axis, and  $Z$  axis, so that the origin  $O_b$  of the ICS coincides with the origin  $O_a$  of the BCS to obtain the translation transformation matrix  $T$ :

$$T = [x \quad y \quad z]^T \tag{2}$$

where  $x$ ,  $y$ , and  $z$  are the displacements of the BCS relative to the  $X$ ,  $Y$ , and  $Z$  axes of the ICS, respectively.

The ICS is rotated in the order around the  $X$  axis,  $Y$  axis, and  $Z$  axis, so that the coordinate axes of the ICS and the BCS are completely coincident to obtain the rotation transformation matrix  $R$ :

$$R = \begin{bmatrix} c\gamma c\psi & c\gamma s\psi s\varphi - s\gamma c\varphi & s\gamma s\varphi + c\varphi c\gamma s\psi \\ s\gamma c\psi & c\gamma c\varphi - s\varphi s\gamma s\psi & s\gamma s\psi c\varphi - c\gamma s\varphi \\ -s\psi & c\psi s\varphi & c\psi c\varphi \end{bmatrix} \tag{3}$$

where  $s$  represents the sine function  $\sin x$ ;  $c$  represents the cosine function  $\cos x$ ;  $\varphi$ ,  $\psi$ , and  $\gamma$  are the rotation angles of the BCS relative to the  $X$ ,  $Y$ , and  $Z$  axes of the ICS, respectively.

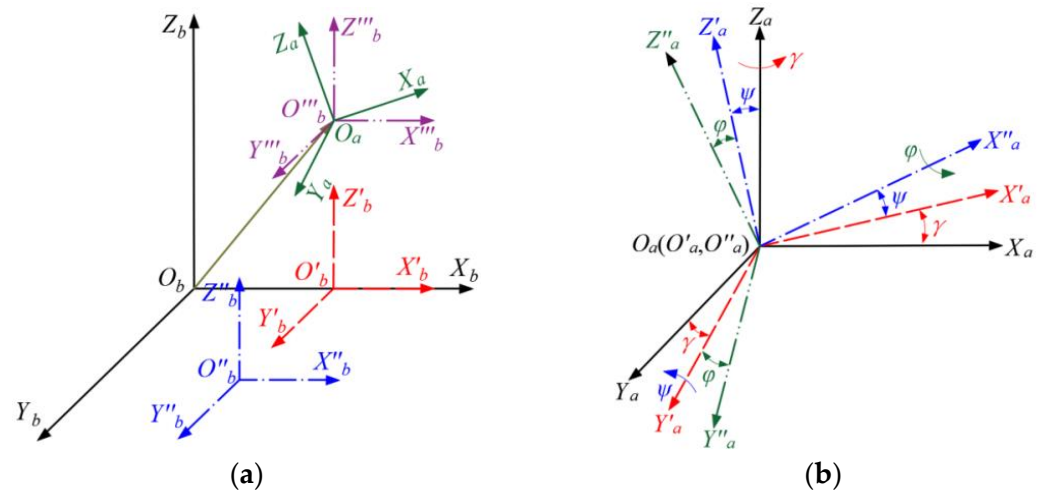


**Figure 4.** Coordinate transformation diagram of the 6-UPS parallel mechanism: (a) Schematic diagram of translation; (b) Schematic diagram of rotation.

Let  $A_i$  be the absolute coordinates of the spherical hinge on the mobile platform and  $B_i$  be the absolute coordinates of the universal joint on the fixed platform, then

$$\begin{cases} A_i = [x_{ia} & y_{ia} & z_{ia}]^T \\ B_i = [x_{ib} & y_{ib} & z_{ib}]^T \end{cases} \quad (i = 1, 2, \dots, 6) \tag{4}$$

Substitute into Formula (1) to obtain

$$\mathbf{L}_i = \begin{bmatrix} l_{ix} \\ l_{iy} \\ l_{iz} \end{bmatrix} = \begin{bmatrix} c\gamma c\psi x_{ia} + (c\gamma s\psi s\varphi - s\gamma c\varphi)y_{ia} + (s\gamma s\varphi + c\varphi c\gamma s\psi)z_{ia} + E_{ix} - x_{ib} \\ s\gamma c\psi x_{ia} + (c\gamma c\varphi - s\varphi s\gamma s\psi)y_{ia} + (s\gamma s\psi c\varphi - c\gamma s\varphi)z_{ia} + E_{iy} - y_{ib} \\ -s\psi x_{ia} + c\psi s\varphi y_{ia} + c\psi c\varphi z_{ia} + E_{iz} - z_{ib} \end{bmatrix} \quad (i = 1, 2, \dots, 6) \tag{5}$$

Add a multi-DOF drive at the center  $O_a$  of the mobile platform of the 6-UPS parallel mechanism; the translational drive along the  $X$ ,  $Y$ , and  $Z$  axes is  $T_x = T_y = T_z = 60 \sin(0.5\pi t)$ , and the rotational drive around the  $X$ ,  $Y$ , and  $Z$  axes is  $R_x = R_y = R_z = 0$ .

Substituting the values into  $l_i = \sqrt{l_{ix}^2 + l_{iy}^2 + l_{iz}^2}$ , the theoretical variation curve of the displacement of each drive branch chain is obtained by solving. The simulation and theoretical comparison results of each drive branch chain are shown in Figure 5.

As can be seen from Figure 5, the simulation results of the displacement of each drive branch chain in the 6-UPS parallel mechanism basically match the theoretical calculation results, and the curve is smooth without sudden change, although there is a certain error, but the maximum error is 1.65%, and the motion trend and direction of both are highly consistent, thus verifying the validity and accuracy of the parameterized model.

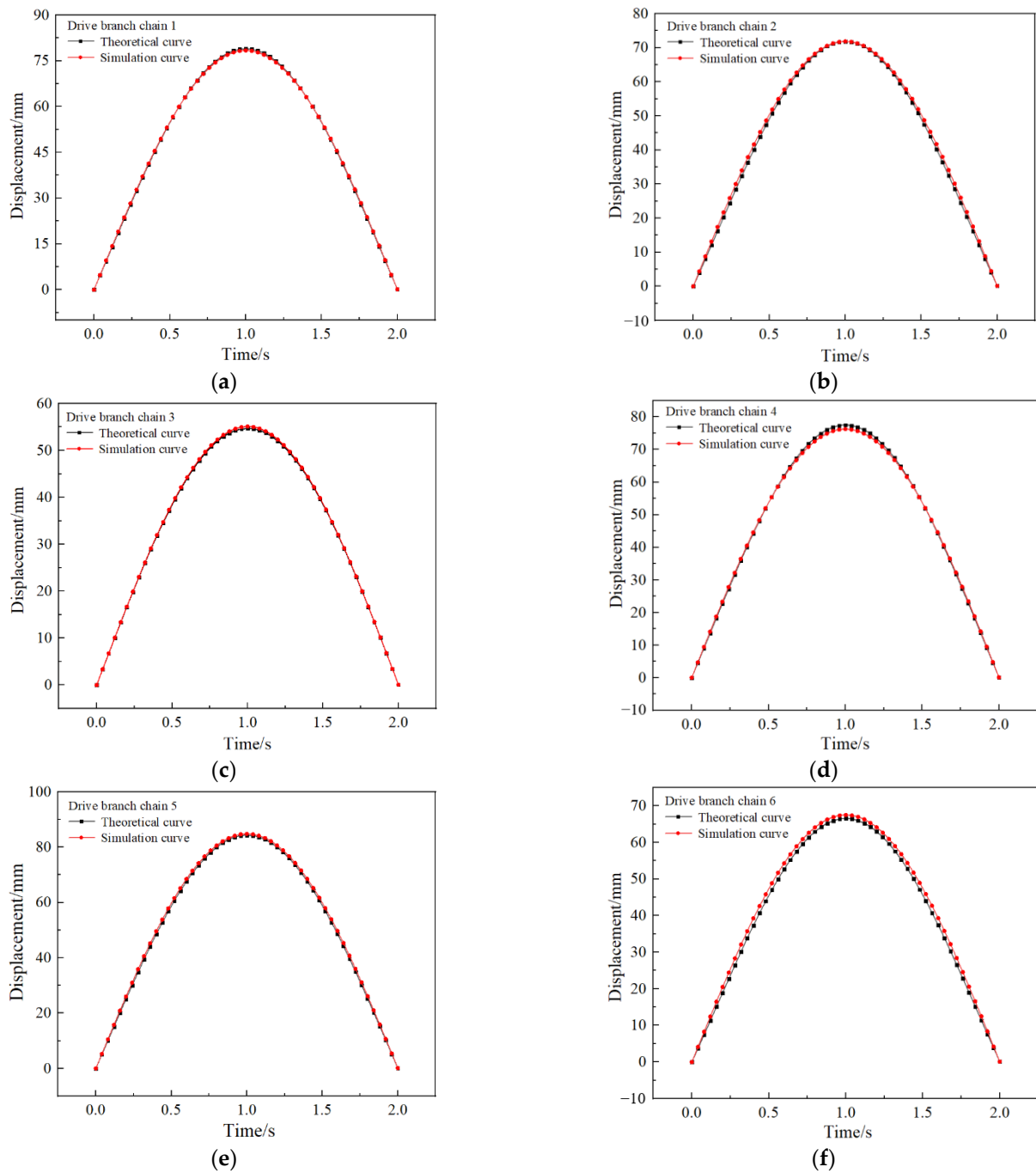


**Figure 5.** Theoretical verification results of the drive branch chain: (a) Drive branch chain 1; (b) Drive branch chain 2; (c) Drive branch chain 3; (d) Drive branch chain 4; (e) Drive branch chain 5; (f) Drive branch chain 6.

#### 4. Mathematical Model for Optimal Design

##### 4.1. Design Variable Creation

According to the actual application purpose of the 6-UPS parallel mechanism, the expected load-bearing capacity and the expected operating space, and other requirements, the design variables of the 6-UPS parallel mechanism are expressed as

$$x = (x_1, x_2, x_3, x_4, x_5)^T = (r, R, \alpha, \beta, H)^T \tag{6}$$

where  $x_i$  ( $i = 1, 2, \dots, 5$ ) is the design variable;  $r$  is the distribution circle radius of the geometric center of the spherical hinge of the mobile platform;  $R$  is the distribution circle radius of the geometric center of the universal joint of the fixed platform;  $\alpha$  is the central angle corresponding to the long side of the spherical hinge;  $\beta$  is the central angle corresponding to the short side of the universal joint;  $H$  is the initial height between the center point Oa of the mobile platform and the center point Ob of the fixed platform.

In Formula (6), the design variables are independent of each other, and the value range of the design variables is shown in Table 2.

**Table 2.** Value range of design variables.

Design Variable	Symbol	Unit	Initial Value	Lower Value	Upper Value
$x_1$	$r$	mm	600	500	700
$x_2$	$R$	mm	850	800	1000
$x_3$	$\alpha$	(°)	90	80	95
$x_4$	$\beta$	(°)	25	20	35
$x_5$	$H$	mm	1000	950	1100

#### 4.2. Objective Function Creation

In order to improve the load-bearing capacity of the 6-UPS parallel mechanism and expand the motion range of the mechanism, this article takes the peak force on the drive pair of the drive branch chain, the minimum value of the projection angle of the BCS relative to the ICS, and the minimum value of the average projected angle of the BCS relative to the ICS is used as the optimization objectives, that is, when the load on the mobile platform is identical to the movement law of the six drive branch chain, the peak force on the drive pair of the six drive branch chain is the smallest, and the minimum value of projected angle and the average projected angle of the BCS relative to the ICS are the largest.

Therefore, the objective function of the multi-objective optimization design of the 6-UPS parallel mechanism is

$$\begin{cases} F(x) = \{\min f_1(x), \max f_2(x), \max f_3(x)\} \\ f_1(x) = \max(F_1, F_2, F_3, F_4, F_5, F_6) \\ f_2(x) = \min(|\varphi|, |\psi|, |\gamma|) \\ f_3(x) = \min\left(\frac{(|\varphi|) + (|\psi|) + (|\gamma|)}{3}\right) \end{cases} \quad (7)$$

where  $f_1(x)$  is the peak force on the drive pair of the drive branch chain;  $f_2(x)$  is the minimum value of the projection angle of the BCS relative to the ICS;  $f_3(x)$  is the minimum value of the average projected angle of the BCS relative to the ICS;  $F_1 \sim F_6$  are the force values of the drive pair of each drive branch chain;  $\varphi$ ,  $\psi$ , and  $\gamma$  are the rotation angles of the BCS relative to the X, Y, and Z axes of the ICS, respectively.

#### 4.3. Constraint Creation

To better ensure the comprehensive performance of the 6-UPS parallel mechanism in the optimization process, in addition to the objective function, the displacement of the prismatic pair of the drive branch chain, the rotation angle of the spherical pair and the universal pair, and the interference of the drive branch chain are used as constraints in the optimization process.

The telescopic length of the drive branch chain determines the stroke range of the prismatic pair, and the displacement constraint of the prismatic pair is expressed as

$$P_{\min} \leq P_i \leq P_{\max} \quad (8)$$

where  $P_{\min}$  is the minimum displacements allowed by the prismatic pair,  $P_{\min} = -300$  mm;  $P_{\max}$  is the maximum displacements allowed by the prismatic pair,  $P_{\max} = 300$  mm.

The rotation angle  $\theta_i$  of the spherical pair and the universal pair cannot exceed its maximum allowable rotation angle  $\theta_{\max}$ , whose constraint is expressed as

$$\theta_i = \arccos \frac{L_i \cdot (\sigma n_i)}{|L_i|} \leq \theta_{\max} \tag{9}$$

where  $L_i$  is the length vector of the drive branch chain;  $\sigma$  is the attitude of the hinge point relative to the ICS;  $n_i$  is the Z axis vector of the  $i$ th hinge point;  $\theta_{\max}$  is the maximum allowable rotation angle,  $\theta_{\max} = 30^\circ$ .

Due to the physical dimensions of the drive branch chains, interference may occur between the branch chains when the mechanism is in motion. Assuming that each drive branch chain is cylindrical, and its diameter is  $D$ , the constraint that the drive branch chain does not interfere is expressed as

$$D \leq D_i \tag{10}$$

where  $D_i$  is the shortest distance between two adjacent centerlines.

### 5. Effect of Design Variables on the Objective Function

#### 5.1. Motion Law of the Drive Branch Chain

To enable the 6-UPS parallel mechanism to complete the translational movement along the X, Y, and Z axes and the rotational movement around the X, Y, and Z axes in a cycle, the drive values in Table 3 are applied to the prismatic pairs of the six drive branch chains.

**Table 3.** Drive values of the drive branch chains.

Number	Drive Value	Number	Drive Value
Drive branch chain 1	$20 \sin(0.8\pi t)$	Drive branch chain 4	$20 \sin(1.8\pi t)$
Drive branch chain 2	$20 \sin(1.2\pi t)$	Drive branch chain 5	$20 \sin(1.4\pi t)$
Drive branch chain 3	$20 \sin(1.6\pi t)$	Drive branch chain 6	$20 \sin(1.0\pi t)$

#### 5.2. Effect of the Distribution Circle Radius of the Geometric Center of the Spherical Hinge of the Mobile Platform on the Objective Function

The effect of the distribution circle radius of the geometric center of the spherical hinge of the mobile platform on the objective function is studied in ADAMS software. The variation curve of the objective function with the distribution circle radius  $r$  of the geometric center of the spherical hinge of the mobile platform is shown in Figure 6.

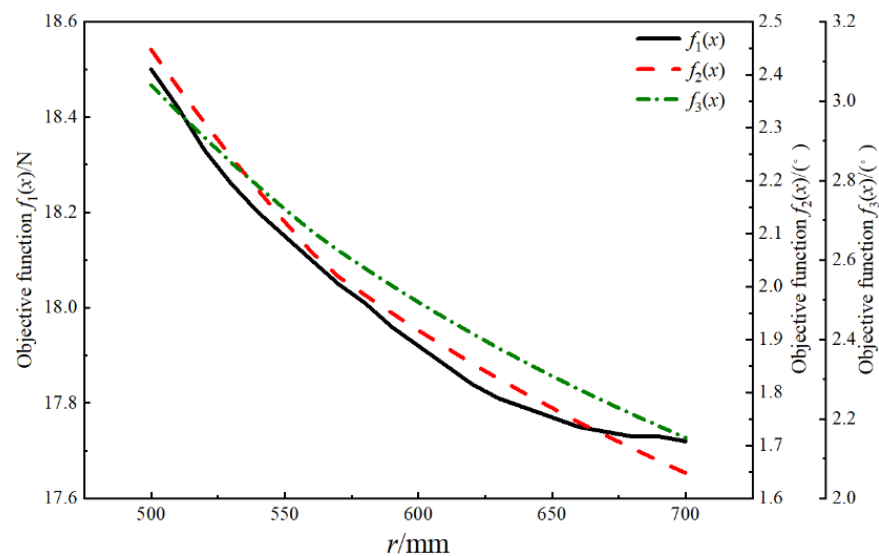


**Figure 6.** Variation curve of the objective function with the distribution circle radius  $r$  of the geometric center of the spherical hinge of the mobile platform.

As can be seen from Figure 6, the objective functions  $f_1(x)$ ,  $f_2(x)$ , and  $f_3(x)$  are negatively correlated with the design variables. With the increase in the distribution circle radius of the geometric center of the spherical hinge of the mobile platform, the performance of the objective function  $f_1(x)$  is gradually enhanced, while the performance of the objective functions  $f_2(x)$  and  $f_3(x)$  is gradually reduced.

5.3. Effect of the Distribution Circle Radius of the Geometric Center of the Universal Joint of the Fixed Platform on the Objective Function

The effect of the distribution circle radius of the geometric center of the universal joint of the fixed platform on the objective function is studied in ADAMS software. The variation curve of the objective function with the distribution circle radius  $R$  of the geometric center of the universal joint of the fixed platform is shown in Figure 7.

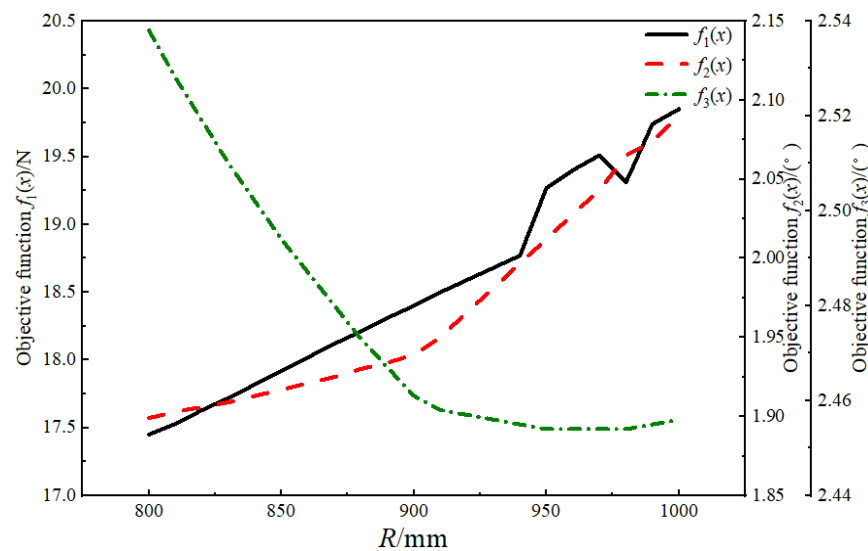


Figure 7. Variation curve of the objective function with the distribution circle radius  $R$  of the geometric center of the universal joint of the fixed platform.

As can be seen from Figure 7, the objective functions  $f_1(x)$  and  $f_2(x)$  are positively correlated with the design variables within a certain range, and the objective function  $f_3(x)$  is negatively correlated with the design variables within a certain range. With the increase in the distribution circle radius of the geometric center of the universal joint of the fixed platform, the performance of the objective functions  $f_1(x)$  and  $f_3(x)$  is gradually reduced, while the performance of the objective function  $f_2(x)$  is gradually enhanced.

5.4. Effect of the Central Angle Corresponding to the Long Side of the Spherical Hinge on the Objective Function

The effect of the central angle corresponding to the long side of the spherical hinge on the objective function is studied in ADAMS software. The variation curve of the objective function with the central angle  $\alpha$  corresponding to the long side of the spherical hinge is shown in Figure 8.

As can be seen from Figure 8, the objective function  $f_1(x)$  is positively correlated with the design variables, and the objective functions  $f_2(x)$  and  $f_3(x)$  are negatively correlated with the design variables. With the increase in the central angle corresponding to the long side of the spherical hinge, the performance of the objective functions  $f_1(x)$ ,  $f_2(x)$ , and  $f_3(x)$  is gradually reduced.

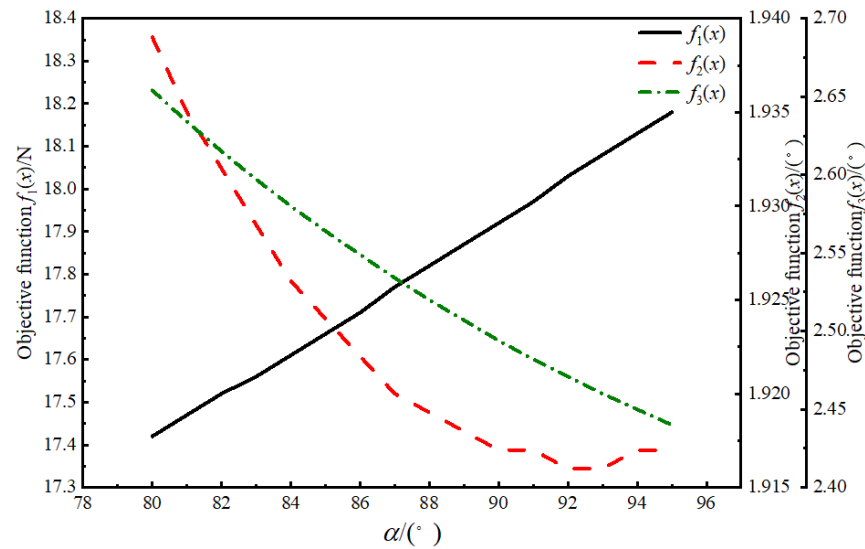


**Figure 8.** Variation curve of the objective function with the central angle  $\alpha$  corresponding to the long side of the spherical hinge.

5.5. Effect of the Central Angle Corresponding to the Short Side of the Universal Joint on the Objective Function

The effect of the central angle corresponding to the short side of the universal joint on the objective function is studied in ADAMS software. The variation curve of the objective function with the central angle  $\beta$  corresponding to the short side of the universal joint is shown in Figure 9.

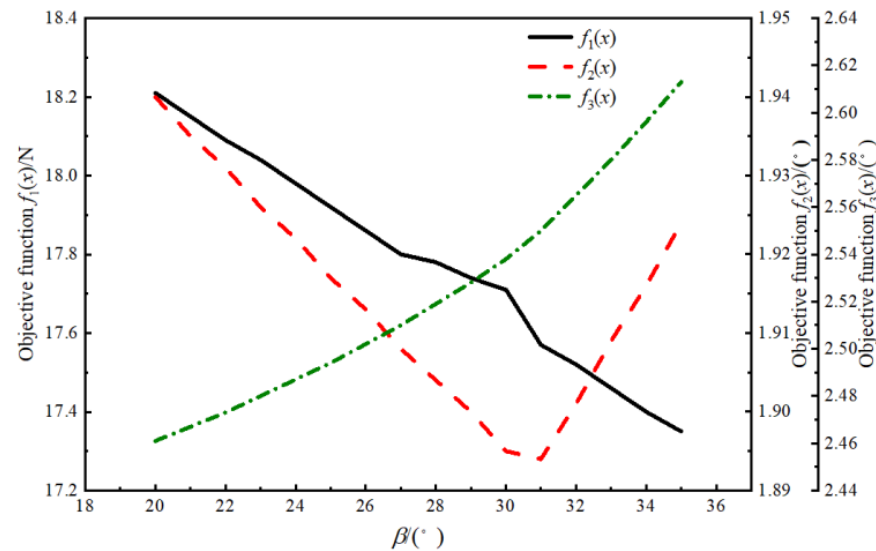


**Figure 9.** Variation curve of the objective function with the central angle  $\beta$  corresponding to the short side of the universal joint.

As can be seen from Figure 9, the objective function  $f_1(x)$  is negatively correlated with the design variables; the objective function  $f_2(x)$  is negatively correlated with the design variables first and is then positively correlated; and the objective function  $f_3(x)$  is positively correlated with the design variables. With the increase in the central angle corresponding to the short side of the universal joint, the performance of the objective functions  $f_1(x)$  and  $f_3(x)$  is gradually enhanced, and the performance of the objective function  $f_2(x)$  is gradually reduced at first and then progressively enhanced.

### 5.6. Effect of the Initial Height between the Mobile and Fixed Platform on the Objective Function

The effect of the initial height between the mobile and fixed platform on the objective function is studied in ADAMS software. The variation curve of the objective function with the initial height  $H$  between the mobile and fixed platform is shown in Figure 10.

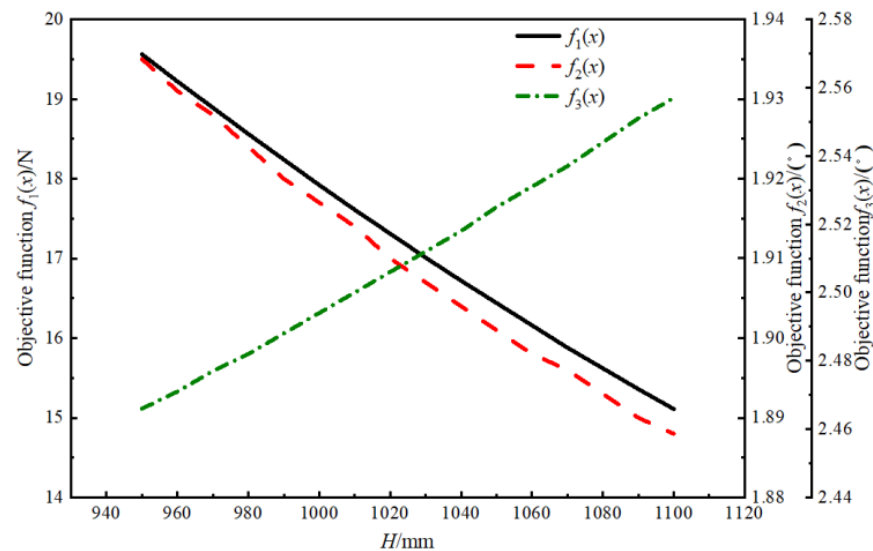


**Figure 10.** Variation curve of the objective function with the initial height  $H$  between the mobile and fixed platform.

As can be seen from Figure 10, the objective functions  $f_1(x)$  and  $f_2(x)$  are negatively correlated with the design variables, and the objective function  $f_3(x)$  is positively correlated with the design variables. As the initial height increases, the performance of the objective functions  $f_1(x)$  and  $f_3(x)$  is gradually enhanced, and the performance of the objective function  $f_2(x)$  is gradually reduced.

## 6. Experimental Scheme Design and Optimization Results Discussion

### 6.1. Experiment Design Based on Taguchi Method

The Taguchi method is an effective mathematical-statistical method, which can mine the information of the whole parameter space through a little number of experiments. The basic steps for using the Taguchi method for experimental design are as follows:

- Identifying the objectives: In the Taguchi method, the specific optimization objective should be defined first, which determines the objective function and influences the classification of variables into controllable factors and noise factors.
- Determining the objective function: Divide the objective function according to three different types: nominally the best, the smaller the better, and the larger the better.
- Selection of controllable factor and noise factor: In the Taguchi method, the controllable factor is determined during the design process, while the noise factor varies according to the conditions of users.
- Selecting an orthogonal array: The orthogonal array can obtain quasi-optimal results without spending a lot of time and uses independent factor impact analysis to reduce computational optimization.
- Simulation and analysis: The analysis phase of the simulation consists of converting the raw data of the objective function into the computation of a representative signal-to-noise ratio, which serves as a measurement tool to determine robustness and is an important factor in optimizing design parameters.

Through the study of the 6-UPS parallel mechanism, five design variables, as shown in Table 2, are determined, which are the main factors affecting the load-bearing capacity and motion range of the mechanism. When different levels of each factor are combined,

the mechanism’s performance will change. Therefore, the optimization of the 6-UPS parallel mechanism is a multi-objective, multi-factor, and multi-level problem. The Taguchi experimental design used in this article includes five factors and four levels  $L_{16} (4^5)$ ; the levels of every factor are shown in Table 4; and the experimental layout and experimental results are shown in Table 5.

**Table 4.** Influencing factors and levels.

Factor	Level 1	Level 2	Level 3	Level 4
$H$	950	1000	1050	1100
$\beta$	20	25	30	35
$\alpha$	80	85	90	95
$R$	800	850	950	1000
$r$	500	600	650	700

**Table 5.** Experimental layout and experimental results.

Number	$H$	$\beta$	$\alpha$	$R$	$r$	$f_1(x)/N$	$f_2(x)/(^{\circ})$	$f_3(x)/(^{\circ})$
1	1	1	1	1	1	19.46	2.441	3.19
2	1	2	2	2	2	19.32	1.95	2.557
3	1	3	3	3	3	20.01	1.845	2.291
4	1	4	4	4	4	20.25	1.706	2.084
5	2	1	2	3	4	18.51	1.694	2.131
6	2	2	1	4	3	18.69	1.926	2.41
7	2	3	4	1	2	17.42	1.879	2.546
8	2	4	3	2	1	18.34	2.595	3.312
9	3	1	3	4	2	18.21	2.047	2.45
10	3	2	4	3	1	18.36	2.541	2.975
11	3	3	1	2	4	15.08	1.609	2.403
12	3	4	2	1	3	14.81	1.713	2.633
13	4	1	4	2	3	15.64	1.774	2.322
14	4	2	3	1	4	14.58	1.655	2.313
15	4	3	2	4	1	17.22	2.945	3.518
16	4	4	1	3	2	15.46	2.248	3.021

### 6.2. Gray Relational Grade

The GRA is a method proposed by Deng [54] in 1982 that uses GRG to represent the grade of approximation between design scheme and ideal scheme, which provides an effective mathematical method for dealing with problems of inadequate information, indigent information, and uncertain information. Due to the order of magnitude difference, the experimental results in Table 5 need to be preprocessed before gray correlation analysis. According to the characteristics of the corresponding data, the experimental results are scaled to between 0 and 1 using the different normalization methods.

If the objective has the feature of ‘bigger is better’, the normalization method is expressed as

$$x_i^*(k) = \frac{x_i(k) - \min_k x_i(k)}{\max_k x_i(k) - \min_k x_i(k)} \tag{11}$$

If the objective has the feature of ‘smaller is better’, the normalization method is expressed as

$$x_i^*(k) = \frac{\max_k x_i(k) - x_i(k)}{\max_k x_i(k) - \min_k x_i(k)} \tag{12}$$

where  $x_i^*(k)$  is the normalized value of the  $i$ th response in the  $k$ th objective function;  $x_i(k)$  is the initial value of the objective function;  $\max_k x_i(k)$  and  $\min_k x_i(k)$  are the maximum and minimum values of the  $k$ th objective function, respectively.

The above normalization method is also called ‘gray generation’, and the corresponding gray relational coefficient (GRC) is calculated as

$$\gamma(x_0^*(k), x_i^*(k)) = \frac{\Delta_{\min} + \zeta \Delta_{\max}}{\Delta_{0i}(k) + \zeta \Delta_{\max}} \tag{13}$$

where  $x_0^*(k)$  is the ideal experimental scheme defined by ideal;  $x_i^*(k)$  is the designed experimental scheme;  $\Delta_{0i}(k)$  is the absolute difference between  $x_0^*(k)$  and  $x_i^*(k)$ ;  $\Delta_{\max}$  and  $\Delta_{\min}$  are the maximum and minimum values of  $\Delta_{0i}(k)$ , respectively;  $\zeta$  is the discrimination coefficient,  $\zeta \in [0, 1]$ .

In this article,  $x_0^*(k) = 1$  is selected as the reference result, and the GRC of the experimental results is shown in Table 6.

**Table 6.** The GRC of experimental results.

Number	Gray Relational Generation			GRC		
	$f_1(x)$	$f_2(x)$	$f_3(x)$	$f_1(x)$	$f_2(x)$	$f_3(x)$
References	1.0000	1.0000	1.0000	1.0000	1.0000	1.0000
[1]	0.1393	0.6228	0.7713	0.3675	0.5700	0.6862
[2]	0.1640	0.2552	0.3298	0.3743	0.4017	0.4273
[3]	0.0423	0.1766	0.1444	0.3430	0.3778	0.3688
[4]	0.0000	0.0726	0.0000	0.3333	0.3503	0.3333
[5]	0.3069	0.0636	0.0328	0.4191	0.3481	0.3408
[6]	0.2751	0.2373	0.2273	0.4082	0.3960	0.3929
[7]	0.4991	0.2021	0.3222	0.4996	0.3852	0.4245
[8]	0.3369	0.7380	0.8563	0.4299	0.6562	0.7768
[9]	0.3598	0.3278	0.2552	0.4385	0.4265	0.4017
[10]	0.3333	0.6976	0.6213	0.4286	0.6231	0.5690
[11]	0.9118	0.0000	0.2225	0.8501	0.3333	0.3914
[12]	0.9594	0.0778	0.3828	0.9249	0.3516	0.4475
[13]	0.8131	0.1235	0.1660	0.7279	0.3632	0.3748
[14]	1.0000	0.0344	0.1597	1.0000	0.3412	0.3731
[15]	0.5344	1.0000	1.0000	0.5178	1.0000	1.0000
[16]	0.8448	0.4783	0.6534	0.7631	0.4894	0.5906

The GRG is calculated by weighted summation of the GRC of each objective function, and the calculation formula of GRG is

$$\Gamma(x_0^*, x_i^*) = \sum_{k=1}^n \omega_k \gamma(x_0^*(k), x_i^*(k)) \tag{14}$$

where  $n$  is the number of objective functions;  $\omega_k$  is the weight coefficient of the  $k$ th objective function,  $\sum_{k=1}^n \omega_k = 1$ .

Usually, since the importance of each objective response may be different, their weights can be calculated by the information entropy representing the uncertainty degree of the random variable, and the information entropy of the  $k$ th objective function is as follows:

$$e_k = -\frac{1}{\ln m} \sum_{i=1}^m \left[ \frac{x_{ik}}{\sum_{i=1}^m x_{ik}} \cdot \ln \frac{x_{ik}}{\sum_{i=1}^m x_{ik}} \right] \tag{15}$$

where  $m$  is the number of responses,  $i = 1, 2, \dots, m$ ;  $n$  is the number of objective functions,  $k = 1, 2, \dots, n$ ;  $x_{ik}$  is the normalized value of the  $i$ th response in the  $k$ th objective function.

The weight coefficient of the objective function can be calculated as

$$\omega_k = \frac{d_k}{\sum_{k=1}^n d_k} \tag{16}$$

where  $d_k$  is the degree of deviation of the  $k$ th objective function,  $d_k = 1 - e_k$ .

The weights of the objective functions  $f_1(x)$ ,  $f_2(x)$ , and  $f_3(x)$  are obtained through calculation as 0.36, 0.32, and 0.32, respectively. The GRG and ranking of each experimental result are shown in Table 7.

**Table 7.** The GRG and ranking of experimental results.

Number	GRG	Ranking
1	0.5343	8
2	0.4000	12
3	0.3624	15
4	0.3387	16
5	0.3713	14
6	0.3994	13
7	0.4390	10
8	0.6133	3
9	0.4229	11
10	0.5358	7
11	0.5379	6
12	0.5887	4
13	0.4982	9
14	0.5886	5
15	0.8264	1
16	0.6203	2

The greater the GRG, the closer the design parameters are to the best combination. Therefore, it can be seen from Table 7 that the 15th experiment among the 16 experiments provides the optimal solution for the multi-objective optimization problem of 6-UPS parallel mechanism.

### 6.3. Factor Effect Analysis

In GRA, the average GRG of each factor level is a significant indicator to determine the best combination of design parameters. The GRG is classified according to the identical level of each column of design parameters in the Taguchi array, and the average GRG is calculated for each factor at the same level.

Taking the average GRG of each level of the  $\alpha$  factor as an example, the third column in Table 5 shows that the factor  $\alpha$  level in the 1st, 6th, 11th, and 16th experiments performed is level 1, and the corresponding value of GRG is the result listed in Table 7. For level 1 of factor  $\alpha$ , the GRG of the 1st, 6th, 11th, and 16th experiments are 0.5343, 0.3994, 0.5379, and 0.6203, respectively. Therefore, the level 1 ( $\alpha_1$ ) average GRG of factor  $\alpha$  is

$$\alpha_1 = (0.5343 + 0.3994 + 0.5379 + 0.6203) / 4 = 0.5229 \tag{17}$$

Similarly, the average GRG of  $\alpha_2$ ,  $\alpha_3$ , and  $\alpha_4$  are 0.5466, 0.4968, and 0.4529, respectively. The same method is used to calculate all average GRG for each factor level, and the calculation results are shown in Table 8.

**Table 8.** Average GRG.

Factor	Level 1	Level 2	Level 3	Level 4	Max-Min
$H$	0.4089	0.4558	0.6411	0.7981	0.3892
$\beta$	0.4567	0.4810	0.5414	0.5403	0.0847
$\alpha$	0.5229	0.5466	0.4968	0.4529	0.0937
$R$	0.5377	0.5124	0.4725	0.4969	0.0652
$r$	0.6275	0.4706	0.4622	0.4591	0.1684

As can be seen from Table 8, the maximum values of the average GRG of the factors  $H$ ,  $\beta$ ,  $\alpha$ ,  $R$ , and  $r$  are  $H_4$ ,  $\beta_3$ ,  $\alpha_2$ ,  $R_1$ , and  $r_1$ , respectively. Therefore, the performance of the

mechanism is optimal when the structural parameters of the 6-UPS parallel mechanism  $H = 1100$  mm,  $\beta = 30^\circ$ ,  $\alpha = 85^\circ$ ,  $R = 800$  mm, and  $r = 500$  mm. In addition, in Table 8, the absolute deviation between the maximum and minimum value of the average GRG of factor  $H$  is the largest. Therefore, factor  $H$  has the most excellent effect on the load-bearing capacity and motion range of the 6-UPS parallel mechanism, followed by factors  $r$ ,  $\alpha$ ,  $\beta$ , and  $R$ .

The effects of different levels of each factor on the multi-objective performance are shown in Figure 11. From the slopes of each factor curve in Figure 11, it can be seen that the initial height  $H$  between the mobile and fixed platform has a positive effect on the performance of the 6-UPS parallel mechanism; the distribution circle radius  $r$  of the geometric center of the spherical hinge of the mobile platform has a negative effect on the performance of the 6-UPS parallel mechanism, while other factors have an uncertain effect on the performance of the 6-UPS parallel mechanism.

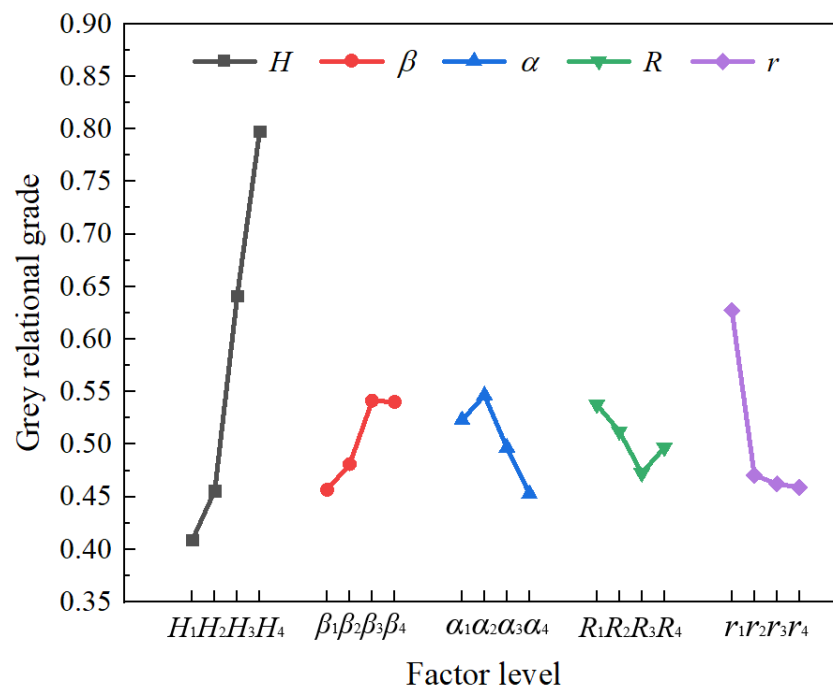
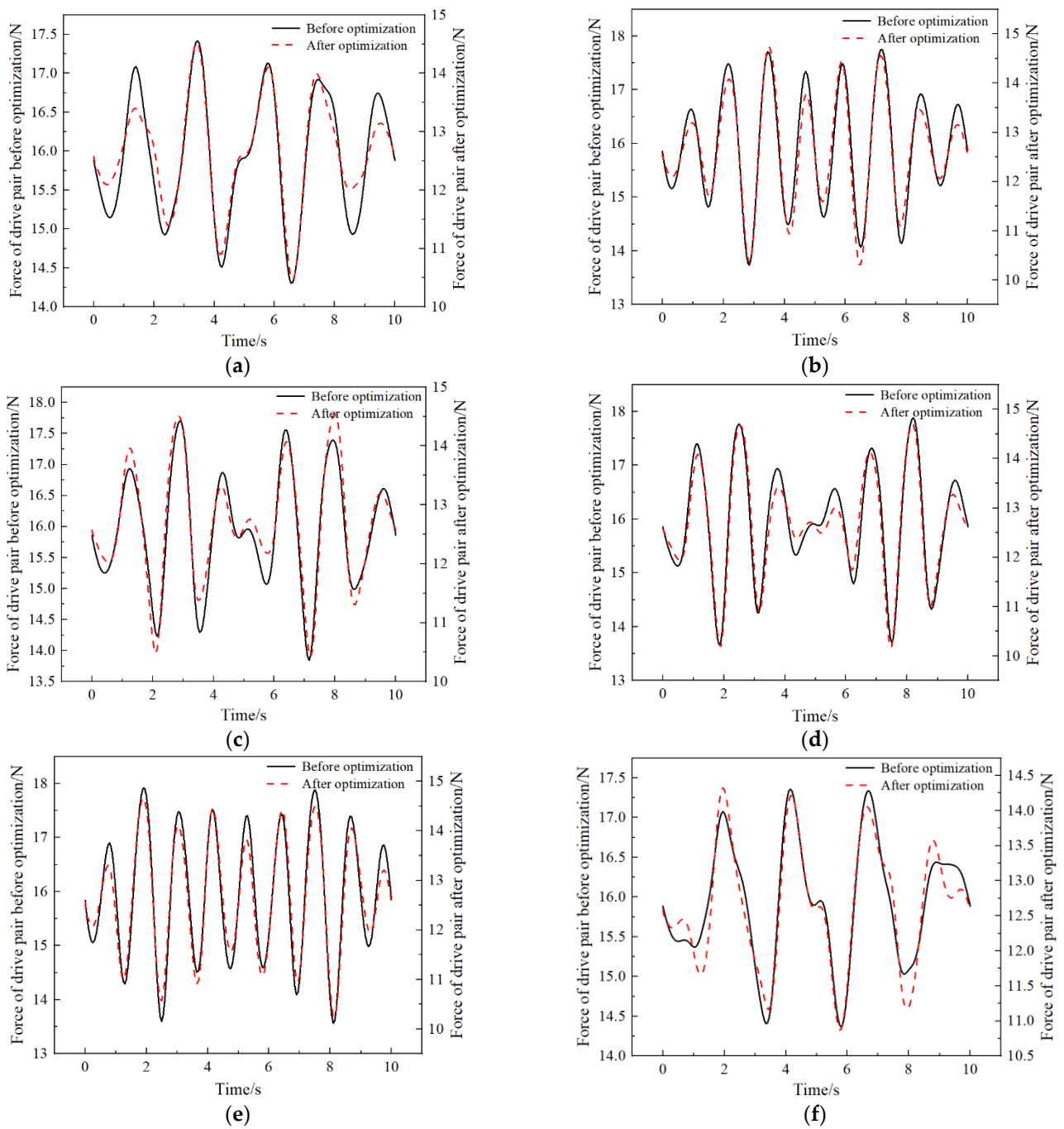


Figure 11. Effect of factor level on multi-objective performance.

#### 6.4. Discussion of Optimization Results

Based on the optimized combination of design parameters, the multi-objective optimized design of the 6-UPS parallel mechanism is completed. Verify the effectiveness of the optimized design by comparing the mechanism’s performance before and after optimization. The force on the drive pair of the six drive branch chains before and after optimization is shown in Figure 12.

It can be seen from Figure 12a–f that the force change trend of the drive pair of the six drive branch chains before and after optimization has a good consistency, and the peak force on the drive pair of each drive branch chain is significantly reduced after optimization. Before and after the optimization design, the peak force on the drive pair of the drive branch chain is shown in Table 9. Combined with Figure 12a–f, the peak force on the drive pair before the optimization of the 6-UPS parallel mechanism appears at the drive branch chain 5, which is 17.922 N; the peak force on the drive pair after optimization appears at the drive branch chain 2, which is 14.744 N, and the improvement rate reaches 17.73%.



**Figure 12.** Force on the drive pair of the six drive branch chains before and after optimization: (a) Drive branch chain 1; (b) Drive branch chain 2; (c) Drive branch chain 3; (d) Drive branch chain 4; (e) Drive branch chain 5; (f) Drive branch chain 6.

**Table 9.** The peak force on the drive pair of the drive branch chain.

Project	Peak Force before Optimization/N	Peak Force after Optimization/N	Improvement Rate/%
Drive branch chain 1	17.418	14.514	16.67
Drive branch chain 2	17.753	14.744	16.95
Drive branch chain 3	17.703	14.532	17.91
Drive branch chain 4	17.885	14.690	17.86
Drive branch chain 5	17.922	14.667	18.16
Drive branch chain 6	17.359	14.323	17.49

The change of the minimum value of the projected angle of the BCS relative to the ICS before and after optimization is shown in Figure 13.

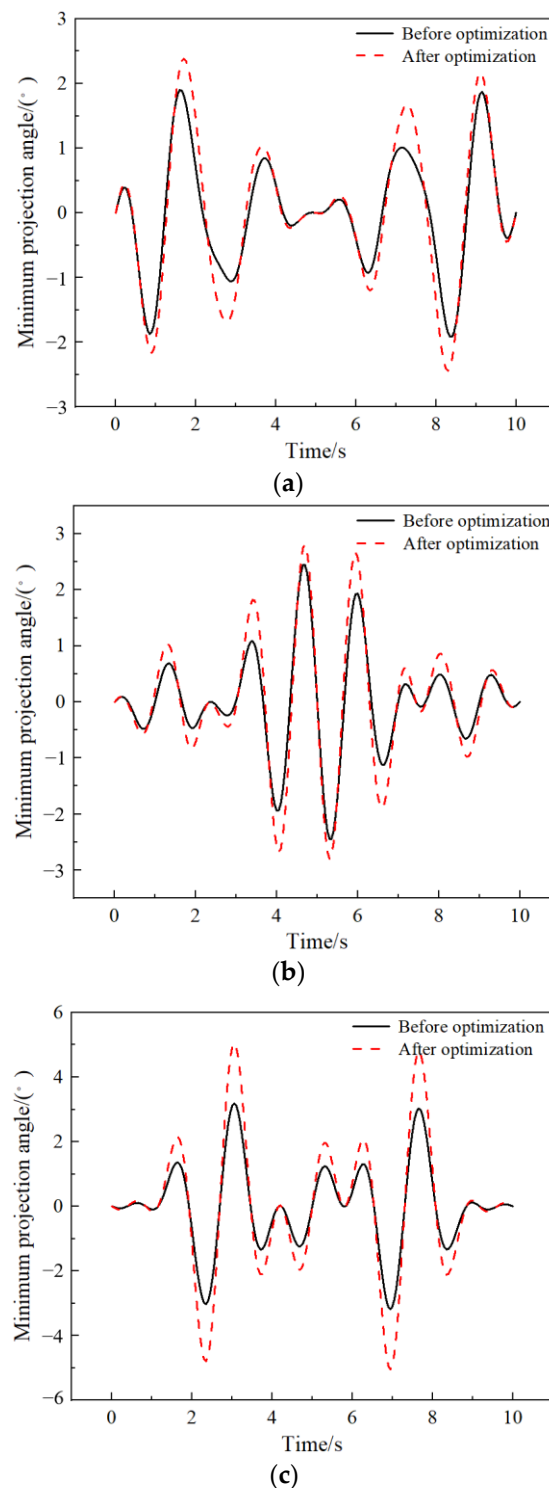


**Figure 13.** Minimum projected angle: (a) X axis; (b) Y axis; (c) Z axis.

It can be seen from Figure 13a–c that the variation trend of the minimum value of the projection angle of the BCS relative to the ICS on the X, Y, and Z axes before and after optimization has a good consistency, and the minimum value of the projection angle and the minimum value of the average projected angle are significantly improved after optimization. Before and after the optimization design, the minimum value of the projection

angle of the BCS relative to the ICS on the X axis is  $1.919^\circ$  and  $2.444^\circ$ , respectively, which appears at 8.35 s and 8.30 s, respectively; the minimum value of the projection angle of the BCS relative to the ICS on the Y axis is  $2.449^\circ$  and  $2.800^\circ$ , respectively, which appears at 4.65 s and 4.70 s, respectively; the minimum value of the projection angle of the BCS relative to the ICS on the Z axis is  $3.188^\circ$  and  $5.048^\circ$ , respectively, both appearing at 6.95 s. Combined with Figure 13a–c, the minimum value of the projection angle before and after optimization of the 6-UPS parallel mechanism is on the X axis, which is  $1.919^\circ$  and  $2.444^\circ$ , respectively, with an improvement rate of 27.36%; the minimum value of the average projected angle before optimization is  $2.519^\circ$ , and after optimization,  $3.430^\circ$ , with an improvement rate of 36.17%.

To reflect more instinctively the motion range before and after optimization of the 6-UPS parallel mechanism, the position parameters of the position vector  $A_i$  at the connection between the mobile platform and the spherical hinge and the position vector  $B_i$  at the connection between the fixed platform and the universal joint in the 6-UPS parallel mechanism are input into the MATLAB software for programming and solving, and the workspace before and after optimization of the 6-UPS parallel mechanism is obtained as shown in Figures 14–17.

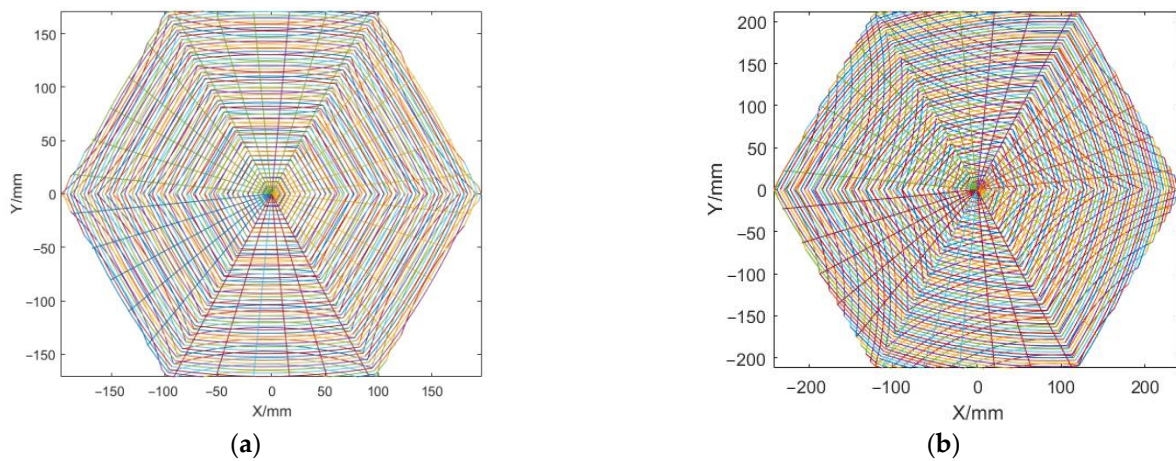


Figure 14. Projection of the workspace on the  $xoy$  plane: (a) Before optimization; (b) After optimization.

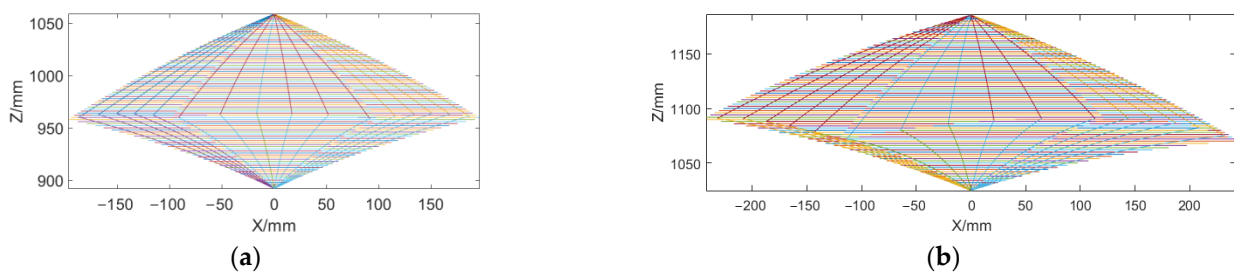


Figure 15. Projection of the workspace on the  $xoz$  plane: (a) Before optimization; (b) After optimization.

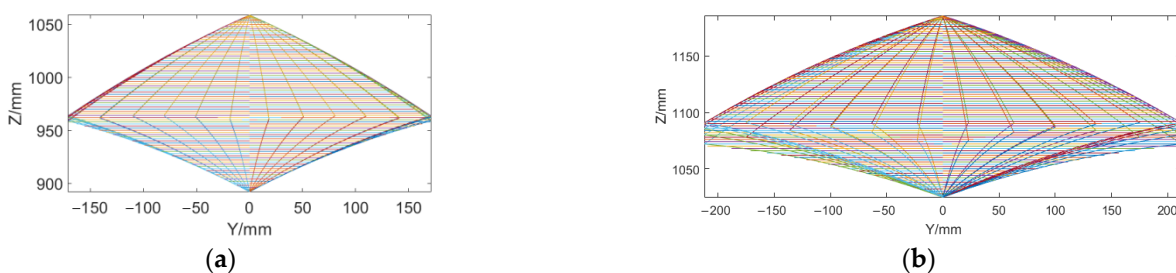
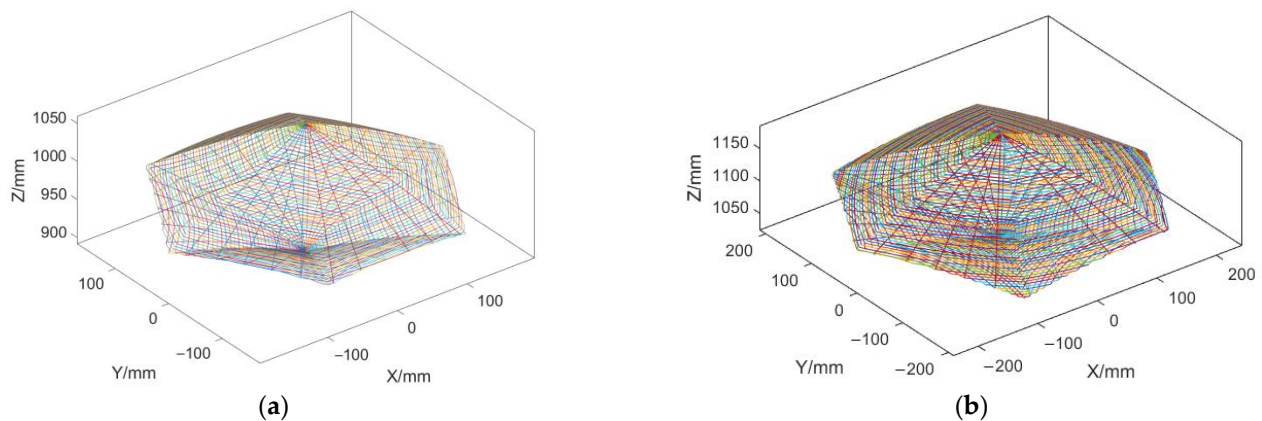


Figure 16. Projection of the workspace on the  $yoz$  plane: (a) Before optimization; (b) After optimization.



**Figure 17.** Three-dimensional distribution of the workspace: (a) Before optimization; (b) After optimization.

It can be seen from Figures 14–17 that the motion range of the optimized 6-UPS parallel mechanism extends to different degrees in the  $X$ ,  $Y$ , and  $Z$  axes, and the motion range in the  $X$  axis is changed from  $[-196.89, 196.89]$  to  $[-242.20, 242.20]$ ; the motion range in the  $Y$  axis is changed from  $[-171.03, 171.03]$  to  $[-212.18, 212.18]$ ; the motion range in the  $Z$  axis is changed from  $[896.91, 1058.93]$  to  $[1021.70, 1185.63]$ , and the motion range of the mechanism is significantly expanded.

## 7. Conclusions

In this article, the multi-objective optimization design of the 6-UPS parallel mechanism is carried out based on the parametric modeling technology, the Taguchi method and EGRA method. The parametric model of the 6-UPS parallel mechanism is established by ADAMS software, and the validity and accuracy of the parametric model are verified by theoretical calculation. The relationship between the design variables and the objective function is investigated by establishing the design variables, objective function, and constraints of the mechanism. Combining the Taguchi method and EGRA method, the multi-objective optimization problem is transformed into a single-objective optimization problem based on the GRG. The best combination of five design variables is determined through factor effect analysis. After the optimized design of the 6-UPS parallel mechanism, the peak force on the drive pair of the drive branch chain is reduced by 17.73%, and the minimum value of the projected angle and the minimum value of the average projected angle of the BCS relative to the ICS are increased by 27.36% and 36.17%, respectively, which significantly improves the load-bearing capacity of the 6-UPS parallel mechanism and expands the motion range of the mechanism.

To sum up, the method proposed in this article attempts to solve multi-objective optimization problems, such as nonlinear and large displacement. Since the multi-objective problem is transformed into a single-objective problem, good results can be obtained when solving nonlinear and complex optimization problems, and computing costs can be significantly reduced. Compared with other multi-objective optimization methods, the method proposed in this article is simpler and more convenient and can be efficiently used in the optimal design of multi-parameter parallel mechanisms, which has certain guiding significance for solving practical engineering problems. In the future, adding more experimental sequences to the experimental design, combining more effective optimization methods, or combining approximate model technology can obtain better optimization results.

**Author Contributions:** Conceptualization, H.S., X.C. and S.Z.; methodology, H.S. and S.Z.; software, H.S.; validation, H.S. and X.C.; formal analysis, H.S., X.C. and S.Z.; writing—original draft preparation, H.S. and X.C.; writing—review and editing, X.C., S.Z. and L.X.; visualization, H.S.; supervision, X.C., S.Z. and L.X.; project administration, S.Z. and L.X.; funding acquisition, S.Z. and L.X. All authors have read and agreed to the published version of the manuscript.

**Funding:** This research was funded by the National Key Research and Development Program of China, grant number 2017YFD070020402; the Key Scientific Research Project of Colleges and Universities in Henan Province, grant number 20A460013; and the Young Talent Support Project in Henan Province, grant number 2020HYTP016.

**Institutional Review Board Statement:** Not applicable.

**Informed Consent Statement:** Not applicable.

**Data Availability Statement:** Not applicable.

**Conflicts of Interest:** The authors declare no conflict of interest.

## References

1. Li, C.Y.; Wu, H.P.; Eskelinen, H. Design and multi-objective optimization of a dexterous mobile parallel mechanism for fusion reactor vacuum vessel assembly. *IEEE Access* **2021**, *9*, 153796–153810. [[CrossRef](#)]
2. Xie, Y.; Li, Y.; Chi, C.F.; Zhu, Z.; Chen, X. Design and analysis of a novel compact XYZ parallel precision positioning stage. *Microsyst. Technol.* **2020**, *27*, 1925–1932. [[CrossRef](#)]
3. Katsushi, F.; Michio, S.; Ryusei, K. Nanometre-cutting machine using a Stewart-platform parallel mechanism. *Meas. Sci. Technol.* **2004**, *15*, 467–474. [[CrossRef](#)]
4. Liu, Y.; Han, X.; Guo, Z.; Jia, X. Structure and kinematics analysis of a novel 4-RPTR parallel mechanism. *China Mech. Eng.* **2010**, *23*, 2812–2815, 2820. [[CrossRef](#)]
5. Kang, D.S.; Seo, T.W.; Kim, J. Development and kinematic calibration for measurement structure of a micro parallel mechanism platform. *J. Mech. Sci. Technol.* **2008**, *22*, 746–754. [[CrossRef](#)]
6. Tang, X.Y.; Chen, I.M.; Li, Q. Design and nonlinear modeling of a large-displacement XYZ flexure parallel mechanism with decoupled kinematic structure. *Rev. Sci. Instrum.* **2006**, *77*, 115101. [[CrossRef](#)]
7. Piccin, O.; Bayle, B.; Maurin, B.; Mathelin, M.D. Kinematic modeling of a 5-DOF parallel mechanism for semi-spherical workspace. *Mech. Mach. Theory* **2009**, *44*, 1485–1496. [[CrossRef](#)]
8. Zhang, D.S.; Xu, Y.D.; Yao, J.T.; Hu, B.; Zhao, Y.S. Kinematics, dynamics and stiffness analysis of a novel 3-DOF kinematically/actuation redundant planar parallel mechanism. *Mech. Mach. Theory* **2017**, *116*, 203–219. [[CrossRef](#)]
9. Wang, S.C.; Hikita, H.; Kubo, H.; Zhao, Y.S.; Huang, Z.; Ifukube, T. Kinematics and dynamics of a 6 degree-of-freedom fully parallel manipulator with elastic joints. *Mech. Mach. Theory* **2003**, *38*, 439–461. [[CrossRef](#)]
10. Monsarrat, B. Singularity analysis of a Three-leg Six-degree-of-freedom parallel platform mechanism based on grassmann line geometry. *Int. J. Robot. Res.* **2001**, *20*, 312–328. [[CrossRef](#)]
11. Kim, J.S.; Park, J.H. Geometric singularity avoidance of a 3-SPS/S parallel mechanism with redundancy using conformal geometric algebra. *J. Korean Soc. Precis. Eng.* **2015**, *32*, 253–261. [[CrossRef](#)]
12. Laryushkin, P.; Glazunov, V.; Erastova, K. On the maximization of joint velocities and generalized reactions in the workspace and singularity analysis of parallel mechanisms. *Robotica* **2019**, *37*, 675–690. [[CrossRef](#)]
13. Nurahmi, L.; Gan, D.M. Reconfiguration of a 3-(rR)PS metamorphic parallel mechanism based on complete workspace and operation mode analysis. *J. Mech. Robot.* **2020**, *12*, 011002. [[CrossRef](#)]
14. Nurahmi, L.; Caro, S.; Wenger, P.; Schadlbauer, J.; Husty, M. Reconfiguration analysis of a 4-RUU parallel manipulator. *Mech. Mach. Theory* **2015**, *96*, 269–289. [[CrossRef](#)]
15. Shen, G.; Li, G.; Zang, W.S.; Li, X.; Tang, Y. Modal space feedforward control for electro-hydraulic parallel mechanism. *IEEE Access* **2019**, *7*, 39751–39761. [[CrossRef](#)]
16. Sun, S.W.; Wu, N.; Zheng, G.; Wang, X.H.; Xia, H.X. Research and implementation on control technology of plane two-DOF dual-truck parallel mechanism. In Proceedings of the 2011 IEEE International Conference on Mechatronics and Automation, Beijing, China, 7–10 August 2011; pp. 1682–1687. [[CrossRef](#)]
17. Huang, G.Y.; Guo, S.; Zhang, D.; Qu, H.B.; Tang, H.Y. Kinematic analysis and multi-objective optimization of a new reconfigurable parallel mechanism with high stiffness. *Robotica* **2017**, *36*, 187–203. [[CrossRef](#)]
18. Wu, M.L.; Zhang, Y.; Yue, X.Q.; Lv, D.Y.; Chen, M.; Wang, X.H.; Zhang, J. Optimal design of an asymmetrical parallel mechanism. *Proc. Inst. Mech. Eng. Part C-J. Eng. Mech. Eng. Sci.* **2021**, *235*, 6922–6939. [[CrossRef](#)]
19. Gao, Z.; Zhang, D. Workspace representation and optimization of a novel parallel mechanism with Three-degrees-of-freedom. *Sustainability* **2011**, *3*, 2217–2228. [[CrossRef](#)]
20. Unnsteinsson, S.D.; Koziel, S. Generalized Pareto ranking bisection for computationally feasible multiobjective antenna optimization. *Int. J. RF Microw. Comput.-Aided Eng.* **2018**, *28*, e21406. [[CrossRef](#)]
21. Liu, Y.; Cheng, Q.S.; Koziel, S. A Generalized SDP Multi-Objective Optimization Method for EM-Based Microwave Device Design. *Sensors* **2019**, *19*, 3065. [[CrossRef](#)]
22. Amrit, A.; Leifsson, L.; Koziel, S. Fast Multi-Objective Aerodynamic Optimization Using Sequential Domain Patching and Multifidelity Models. *J. Aircr.* **2020**, *57*, 388–398. [[CrossRef](#)]
23. Qi, Y.; Sun, T.; Song, Y.M. Multi-objective optimization of parallel tracking mechanism considering parameter uncertainty. *J. Mech. Robot.* **2018**, *10*, 041006. [[CrossRef](#)]

24. Zhang, H.Q.; Tang, J.L.; Gao, Q.; Cui, G.H.; Shi, K.; Yao, Y.A. Multi-objective optimization of a redundantly actuated parallel robot mechanism for special machining. *Mech. Sci.* **2022**, *13*, 123–136. [[CrossRef](#)]
25. Mirshekari, E.; Ghanbarzadeh, A.; Shirazi, K.H. Structure comparison and optimal design of 6-RUS parallel manipulator based on kinematic and dynamic performances. *Lat. Am. J. Solids Struct.* **2016**, *13*, 2414–2438. [[CrossRef](#)]
26. Liu, X.J.; Wang, J.S. A new methodology for optimal kinematic design of parallel mechanisms. *Mech. Mach. Theory* **2007**, *42*, 1210–1224. [[CrossRef](#)]
27. Pan, Y.J.; Hou, L. Lifting and parallel lifting optimization by using sensitivity and fuzzy set for an earthmoving mechanism. *Proc. Inst. Mech. Eng. Part D-J. Automob. Eng.* **2016**, *231*, 192–203. [[CrossRef](#)]
28. Wang, L.P.; Xu, H.Y.; Guan, L.W. Optimal design of a 3-PUU parallel mechanism with 2R1T DOFs. *Mech. Mach. Theory* **2017**, *114*, 190–203. [[CrossRef](#)]
29. Pietrenko-Dabrowska, A.; Koziel, S. Nested Kriging Surrogates for Rapid Multi-Objective Optimization of Compact Microwave Components. *Appl. Comput. Electromagn. Soc. J.* **2021**, *35*, 1344–1345. [[CrossRef](#)]
30. Koziel, S.; Pietrenko-Dabrowska, A. Fast Multi-Objective Optimization of Antenna Structures by Means of Data-Driven Surrogates and Dimensionality Reduction. *IEEE Access* **2020**, *8*, 183300–183311. [[CrossRef](#)]
31. Koziel, S.; Pietrenko-Dabrowska, A. Rapid multi-objective optimization of antennas using nested kriging surrogates and single-fidelity EM simulation models. *Eng. Comput.* **2020**, *37*, 1491–1512. [[CrossRef](#)]
32. Villiers, D.; Koziel, S.M. Fast multi-objective optimisation of pencil beam reflector antenna radiation pattern responses using Kriging. *IET Microw. Antennas Propag.* **2018**, *12*, 120–126. [[CrossRef](#)]
33. Pietrenko-Dabrowska, A.; Koziel, S. Accelerated multiobjective design of miniaturized microwave components by means of nested kriging surrogates. *Int. J. RF Microw. Comput.-Aided Eng.* **2020**, *30*, e22124. [[CrossRef](#)]
34. Koziel, S.; Pietrenko-Dabrowska, A. Tolerance-Aware Multi-Objective Optimization of Antennas by Means of Feature-Based Regression Surrogates. *IEEE Trans. Antennas Propag.* **2022**; early access. [[CrossRef](#)]
35. Hu, Y.; Li, B. Robust design and analysis of 4PUS-1RPU parallel mechanism for a five-degree-of-freedom hybrid kinematic machine. *Proc. Inst. Mech. Eng. Part B-J. Eng. Manuf.* **2011**, *225*, 685–698. [[CrossRef](#)]
36. Stufken, J. Taguchi methods: A hands on approach. *Technometrics* **1994**, *36*, 121–122. [[CrossRef](#)]
37. Ouyang, P.R. A spatial hybrid motion compliant mechanism: Design and optimization. *Mechatronics* **2011**, *21*, 479–489. [[CrossRef](#)]
38. Kim, D.; Hong, H.; Kim, H.S.; Kim, J. Optimal design and kinetic analysis of a stair-climbing mobile robot with rocker-bogie mechanism. *Mech. Mach. Theory* **2012**, *50*, 90–108. [[CrossRef](#)]
39. Park, S.; Kim, J.; Jeong, J.I.; Kim, J.; Lee, G. Optimal dimensioning of redundantly actuated mechanism for maximizing energy efficiency and workspace via Taguchi method. *Proc. Inst. Mech. Eng. Part C-J. Eng. Mech. Eng. Sci.* **2018**, *231*, 326–340. [[CrossRef](#)]
40. Wu, C.Q.; Wu, Y.F. Robust optimal design of compliant parallel robot for the complex multiple response problems. In Proceedings of the 3rd Asian Pacific Conference on Mechanical Components and Control Engineering, Tianjin, China, 20–21 September 2014; Volume 668–669, pp. 518–521. [[CrossRef](#)]
41. Shin, H.; Lee, S.; In, W.; Jeong, J.I.; Kim, J. Kinematic optimization of a redundantly actuated parallel mechanism for maximizing stiffness and workspace using Taguchi method. *J. Comput. Nonlinear Dyn.* **2011**, *6*, 011017. [[CrossRef](#)]
42. Koziel, S.; Pietrenko-Dabrowska, A. Recent advances in accelerated multi-objective design of high-frequency structures using knowledge-based constrained modeling approach. *Knowl.-Based Syst.* **2020**, *214*, 106726. [[CrossRef](#)]
43. Zhang, Y.H.; Liu, C.; Xu, T.T.; Huang, Y.; Tao, L.Y. Impact analysis and classification of aircraft functional failures using improved FHA based on grey evaluation. *Grey Syst.* **2020**, *10*, 159–171. [[CrossRef](#)]
44. Zhang, Z.F.; Li, H.L.; Yue, L.; Du, Y.K. End of life vehicle disassembly plant layout evaluation integrating gray correlation and decision making trial and evaluation laboratory. *IEEE Access* **2020**, *8*, 141446–141455. [[CrossRef](#)]
45. Dao, T.P.; Huang, S.C. Optimization of a two degrees of freedom compliant mechanism using Taguchi method-based grey relational analysis. *Microsyst. Technol.* **2017**, *23*, 4815–4830. [[CrossRef](#)]
46. Huang, S.C.; Dao, T.P. Multi-objective optimal design of a 2-DOF flexure-based mechanism using hybrid approach of Grey-Taguchi coupled response surface methodology and entropy measurement. *Arab. J. Sci. Eng.* **2016**, *41*, 5215–5231. [[CrossRef](#)]
47. Hsieh, C.C.; Hung, C.C.; Hsiao, T.J.; Li, T.C. Finite element analysis applied to the taper mechanism of excavator assembly alignment analysis and optimization. *Eng. Fail. Anal.* **2021**, *121*, 747–752. [[CrossRef](#)]
48. Koziel, S.; Pietrenko-Dabrowska, A. Constrained multi-objective optimization of compact microwave circuits by design triangulation and pareto front interpolation. *Eur. J. Oper. Res.* **2022**, *299*, 302–312. [[CrossRef](#)]
49. Koziel, S.; Sigurdsson, A.T. Multi-fidelity EM simulations and constrained surrogate modelling for low-cost multi-objective design optimisation of antennas. *IET Microw. Antennas Propag.* **2018**, *12*, 2025–2029. [[CrossRef](#)]
50. Shang, J.R.; Tian, Y.N.; Liu, Y.; Liu, R.L. Production scheduling optimization method based on hybrid particle swarm optimization algorithm. *J. Intell. Fuzzy Syst.* **2018**, *34*, 955–964. [[CrossRef](#)]
51. Yildiz, A.R. A novel hybrid whale–Nelder–Mead algorithm for optimization of design and manufacturing problems. *Int. J. Adv. Manuf. Technol.* **2019**, *105*, 5091–5104. [[CrossRef](#)]
52. Wang, D.F.; Xie, C.; Wang, S. An adaptive RBF neural network-based multi-objective optimization method for lightweight and crashworthiness design of cab floor rails using fuzzy subtractive clustering algorithm. *Struct. Multidiscip. Optim.* **2021**, *63*, 915–928. [[CrossRef](#)]

- 
53. Xiong, F.; Wang, D.F.; Ma, Z.D.; Chen, S.M.; Lv, T.T.; Lu, F. Structure-material integrated multi-objective lightweight design of the front end structure of automobile body. *Struct. Multidiscip. Optim.* **2018**, *57*, 829–847. [[CrossRef](#)]
  54. Deng, J.L. Control problems of grey systems. *Syst. Control Lett.* **1982**, *1*, 288–294. [[CrossRef](#)]